ARTICLE

Check for updates

Mesophotic foraminiferal-algal nodules play a role in the Red Sea carbonate budget

Valentina Alice Bracchi [1,2✉], Sam J. Purkis[3], Fabio Marchese[4], Megan K. B. Nolan[4,5], Tullia Isotta Terraneo[4], Silvia Vimercati[4,5], Giovanni Chimienti[2,4], Mattie Rodrigue[6], Ameer Eweida[7] & Francesca Benzoni[4,5]

During two scientific expeditions between 2020 and 2022, direct surveys led to the discovery of free-living mesophotic foraminiferal-algal nodules along the coast of the NEOM region (northern Saudi Arabian Red Sea) where they form an unexpected benthic ecosystem in mesophotic water depths on the continental shelf. Being mostly spheroidal, the nodules are transported *en masse* down slope, into the deep water of the basin, where they stop accreting. Radiometric dating informs that these nodules can be more than two thousand years old and that they collectively contribute up to $66\,g\,m^{-2}\,year^{-1}$ to the mesophotic benthic carbonate budget and account for at least 980 megatons of calcium carbonate, a substantial contribution considering the depauperate production of carbonate by other means in this light-limited environment. Our findings advance the knowledge of mesophotic biodiversity and carbonate production, and provide data that will inform conservation policies in the Saudi Arabian Red Sea.

[1] Department of Earth and Environmental Sciences, University of Milano-Bicocca, Milan, Italy. [2] Consorzio Nazionale Interuniversitario per le Scienze del Mare (CoNISMa), Rome, Italy. [3] Department of Marine Geosciences, Rosenstiel School of Marine and Atmospheric Science, University of Miami, Miami, FL, USA. [4] Red Sea Research Center, King Abdullah University of Science and Technology (KAUST), Thuwal 23955-6900, Saudi Arabia. [5] Marine Science Program, Biological and Environmental Science and Engineering Division, King Abdullah University of Science and Technology (KAUST), Thuwal 23955-6900, Saudi Arabia. [6] OceanX, New York, NY, USA. [7] NEOM, Riyadh, Saudi Arabia. ✉email: valentina.bracchi@unimib.it

Biogenic carbonate nodules are common constituents of modern marine environments. They have been reported worldwide[1,2], and are built by one or more carbonate-producing organisms in approximately concentric layers (Supplementary Note 1). These nodules can form extensive beds on the seafloor, and represent a key component of the marine resources, as they promote and support high biological diversity, among which rhodolith beds are the most widespread and well-documented[2–5]. Moreover, they should be considered for their contribution into carbonate budgets and need to be taken into account for the predictive modeling of the global carbon cycle. The carbonate budget of shallow tropical coral reefs has received increasing attention also in the context of global climate change[6]. Yet, other carbonate factories such as biogenic carbonate nodule beds are less explored, lack quantitative studies, and their temporal dynamics remain unknown[7], especially for the mesophotic zone, i.e., marine environments below the limit of 30 m according to ref. [8] and chapters therein referring to a global scale anthology of reviews.

In the tropics, biogenic carbonate nodules made of Foraminiferal-Algal Nodules (FANs) *sensu* Reid and Macintyre[1] occur from shallow (photic zone) to mesophotic depths[1,9–12]. In the Atlantic, this type of nodule built in variable proportions by concentrically laminated crusts of the encrusting foraminifer *Gypsina* and Crustose Coralline Algae (CCA) is known from Florida's outer shelf (35–65 m)[9], the eastern Caribbean (30–60 m)[1] and the Gulf of Mexico (45–80 m)[10]. In the Pacific Ocean, nodules of encrusting foraminifer *Acervulina* and CCA have been identified on a flat seabed between 61 and 105 m depth in Ryukyu Islands, Japan[11–13].

In the Red Sea, similar nodules have previously been collected at the base of a fringing reef in Dahab Bay (Gulf of Elat/Aqaba, Egypt) between 40 and 60 m depth[14–16]. Encrusting foraminifer *Acervulina inhaerens* Schulze 1845 and CCA mainly generated these spheroidal nodules, coating coral debris with the minor contribution of bryozoans and benthic foraminifers[14–16]. A further record of mesophotic nodules comes from Shambaya Reef (Sudan), where, instead, rhodoliths occur on gently inclined plains at 60 m depth[17].

Characterization and zonation of Red Sea benthic habitats are described for shallow coastal ecosystems and mesophotic coral ecosystems[8,18,19]. Efforts to explore mesophotic and aphotic ecosystems of the Saudi Arabia Red Sea have recently increased[17,20–27], including work on benthic foraminifers[28]. While the country's coastal development presents unprecedented challenges for conservation and management of the marine environment, the knowledge of deeper marine biological resources is still sparse. Among the so-called Saudi giga-projects, NEOM is the most ambitious. Its territory spans the Gulf of Aqaba (GoA) and northeast Red Sea (NERS) coastlines (Fig. 1), thus encompassing part of the known natural variability of oceanographic conditions along the Red Sea marine environment latitudinal gradient[29]. During two scientific expeditions, Remotely Operated Vehicles (ROV) and submersibles surveys led to the discovery of extensive mesophotic biogenic nodule beds (Figs. 2, 3 and Supplementary Table 1) aggregating biological diversity. In this study, we provide the first account of the NEOM foraminiferal-algal nodule spatial and temporal dynamics and evidence that they represent a previously unknown carbonate factory.

Results and discussion
The NEOM mesophotic foraminiferal-algal nodules. The examined nodules ($n = 42$ alive, $n = 3$ dead, Supplementary Table 2) are complex macroids, each supports at least one colony

of the zooxanthellate hard coral genus *Leptoseris* (Fig. 3a, b). Thin living CCA crusts occur at the surface together with encrusting foraminifers, small azooxanthellate corals (e.g., *Polycyathus*), bryozoans, annelids, endolithic mollusks and brachiopods (Fig. 3a, b). Nodules (measured samples $n = 20$, Supplementary Table 2) are of similar size to *pétanque* balls (mean dimensions: $8.1 \times 6.6 \times 5.6$ cm), and typically are partially buried in the sedimentary substrate (Figs. 2–3). The upper, emergent portions of the nodules are colored pink (Fig. 3a), in part due to thin crusts of living CCA, and due to heavy encrustation by various micro and macro-epiphytes organisms including sponges, other macroalgae, gorgonians, black corals and scleractinian corals and encrusting foraminifers (Figs. 2a, b and 3a). The nodules are sub-spheroidal to spheroidal in shape (L = 3.7–12.5 cm; I = 2.8–9.2 cm; S = 2–7.9 cm, Supplementary Table 2) (Fig. 2g). Calculated volumes range between 10.8 and 433.3 cm³ (average volume 173.3 cm³) (Supplementary Table 1). Mass ranges between 23.9 and 544.4 g (average mass 225.9 g) (Supplementary Table 2). Density ranges between 0.9 and 2.2 g cm⁻³ (average density 1.4 g cm⁻³) (Supplementary Table 2). Volume and mass are well correlated (R = 0.9613, Supplementary Table 2), which suggests that the inner features are similar in terms of density and porosity among nodules from different sampling sites. The nodules are built via sequential growth of more or less concentric, both symmetrical and asymmetrical, biogenic carbonate layers (Fig. 3c). Very small particles act as nucleus and are sometimes identifiable (Fig. 3c). Interestingly, these particles are of different nature (Fig. 4c), and in some cases, the same nodule presents more than one particle acting as nucleus, as the results of a coalescence process. Other nodules seem not to have any kind of nucleus (Supplementary Fig. 1). The most abundant builders are encrusting foraminifer (*Acervulina* cf. *inhaerens*, Fig. 3d, e), which form thick layers alternating with thin CCA crusts (Fig. 3d, e), thus we identify the observed nodules as FANs *sensu* 1. The contribution of the other observed taxa to the nodule is negligible, although sometimes annelids are abundant on their outer surface. The inner structure is quite compact (Fig. 3c and Supplementary Fig. 1). Unlithified or lithified biogenic fine sands and muds partially fill voids when present (Fig. 3c, e and Supplementary Fig. 1), or they are occupied by endolithic bivalves (Supplementary Fig. 1).

The NEOM FANs differ from the rhodoliths reported from Sudan, which lack a substantial foraminiferal component[17]. In fact, our FANs are formed by a bioconstructional guild similar to the one building the GoA nodules. These, however, occur at a shallower depth yet[14–16], have a nucleus and are smaller and more porous. The Ryukyu Islands' ones appear to be more similar but with higher porosity[11–13]. Interestingly, in the Atlantic a foralgal factory is reported as forming nodules although the key foraminifer builder is the genus *Gypsina* rather than *Acervulina*[1,9,10].

Radiometric dating reveals that the NEOM FANs date back at least 2362 cal years BP (Supplementary Table 3). The average estimated FAN accretion rate ranges between 0.01 and 0.02 mm yr⁻¹ (Supplementary Table 3). This is the first indication of accretion rate for Red Sea mesophotic nodules and provides a first indication on the nodule development and persistence interval on the seafloor. Only one case of mesophotic sub-tropical FANs was dated so far (2750 BP)[11] with an accretion rate similar to ours, corresponding to 0.02 mm yr⁻¹ [12]. More data exist on other mesophotic nodules, such as rhodoliths, whose accretion rates was quantified from different marine tropical environments[30]. Mesophotic rhodoliths can grow from a minimum of 0.01–0.05 mm/yr (from Bahamas, 67–91 m[31] to a maximum of 0.7 mm yr⁻¹ (Egypt, 3 m)[32]. Data on the growth rate of mesophotic corals are limited only to the Caribbean,
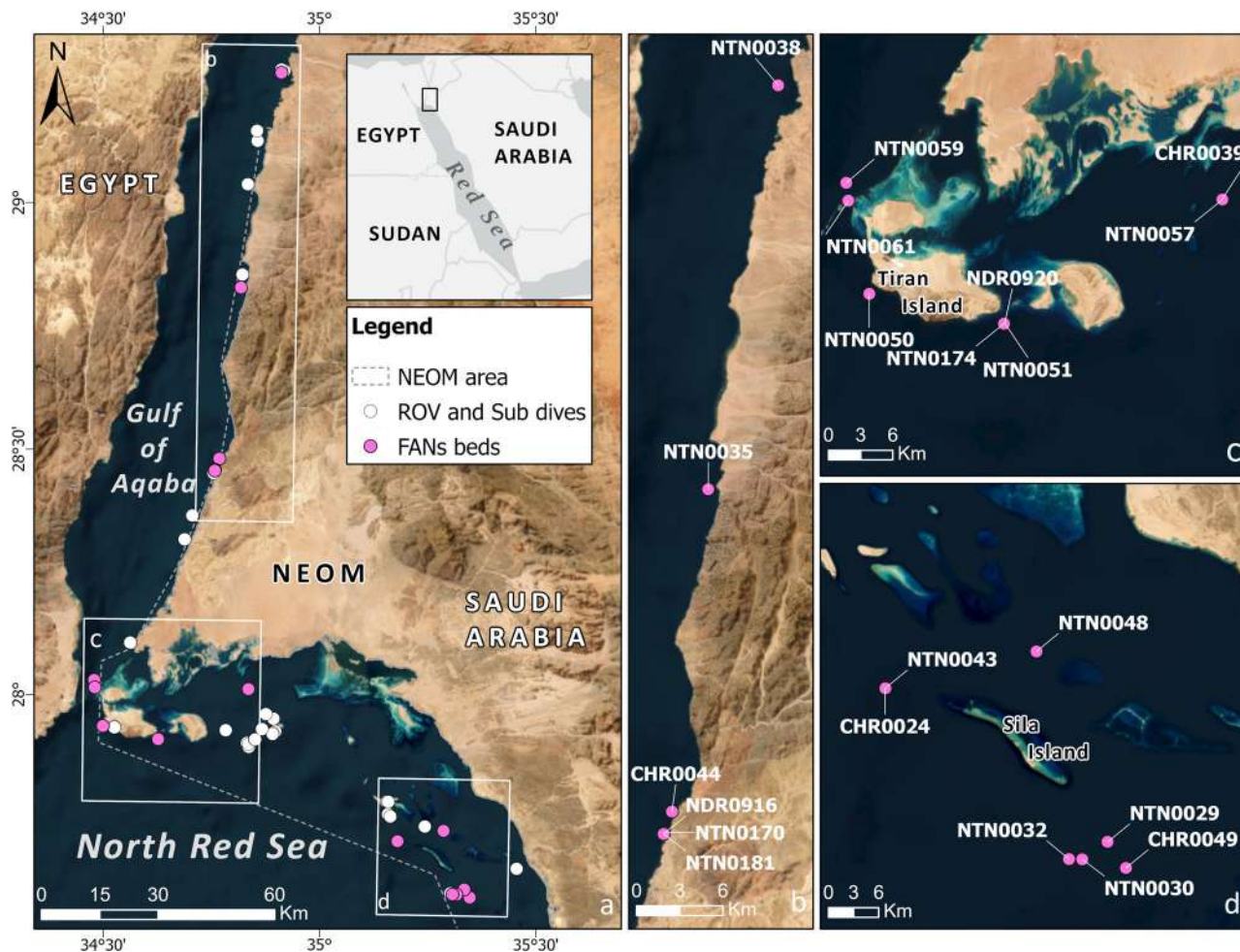
Fig. 1 Map of the study area with the indication of sampling effort. a Map of NEOM region showing remote operated vehicle and submersible video-transects position. Each dot represents a video-transect. Pink dots indicate sites where FANs were observed. White dots indicate survey sites where no FANs were observed either because they did not occur in the depth range or because the transect ended deeper than the FANs occurrence range. **b** Magnification of inset b in (**a**) with details of the sampling sites around Magna, Gulf of Aqaba. **c** Magnification of inset c in (**a**) with details of the sampling sites around Tiran Islands, between the Gulf of Aqaba and NE Red Sea. **d** Magnification of inset d in (**a**) with details of the sampling sites at NE Red Sea. ESRI World Image Basemap, source: Esri, Maxar, Earthstar Geographics.

therefore not significant for our comparison, but generally indicate a slower growth rate for mesophotic, relative to shallow water corals[33,34]. Overall, the available evidence points to a general slow accretion rate of biogenic nodules in mesophotic zones, as expected. The slow, and resilient, accretion rate of NEOM FANs can have important implications in terms of the development and conservation of these ecosystems. Strong disturbances, such as changes in sedimentation rate, or water turbidity, especially in the context of a region where ambitious development projects are underway, can have the potential to be detrimental for their survival. Moreover, considering a long-term dynamic, seawater acidification because of climate change can also be anticipated to influence these bioconstructions by inhibiting accretion. Our results, therefore, contribute to the knowledge of the variability of the Red Sea mesophotic ecosystems and provide specific indications that should be considered for the sustainable development of the region.

The NEOM mesophotic nodule beds. In NEOM, we found FAN beds at 21 out of 38 surveys reaching the mesophotic zone (Figs. 1, 2 and Supplementary Table 1), between 43 and 132 m water depth (wd). Their distribution never extends into the photic zone, when we reached it (Supplementary Table 1). Considering

the radiocarbon dating we obtained together with the depth range inhabited by the FANs, we can argue that their development is mesophotic within the last 2 kyr and under oceanographic and climate conditions that are similar to the present[35].

Moreover, the bathymetric distribution of the NEOM FAN beds, although restricted to the mesophotic, is not uniform along the shelf (Fig. 4a and Supplementary Table 1). The FANs beds are sometimes found within a very narrow bathymetric interval (90.5–92 m wd, CHR0049), whereas along other transects their range is wider (57.3–117.8 m wd, NTN0181) and/or shallower (58.6–98.5 m wd, NTN0043) or deeper (114.2–131.8 m wd, NTN0032) (Fig. 4a and Supplementary Table 1).

FANs covered the seafloor in variable proportions ranging from 25 to 100% (Fig. 2, Supplementary Table 2) both in the GoA and in the NERS where their deepest occurrence was recorded (Supplementary Table 2). The observed number of FANs *per* square meter ranges between 50 and 287 (Fig. 2e, Supplementary Table 2). At the time of our surveys, nodule beds occurred at relatively homogeneous salinity (40–41 PSU, Fig. 4b, and Supplementary Table 2). However, overall recorded temperature ranges differed between the GoA (21.38–26.59 °C) and the NERS (22.3–28.8 °C) (Fig. 4b, Supplementary Table 2). Oceanographic data collected at the sampling sites (Supplementary Tables 1 and
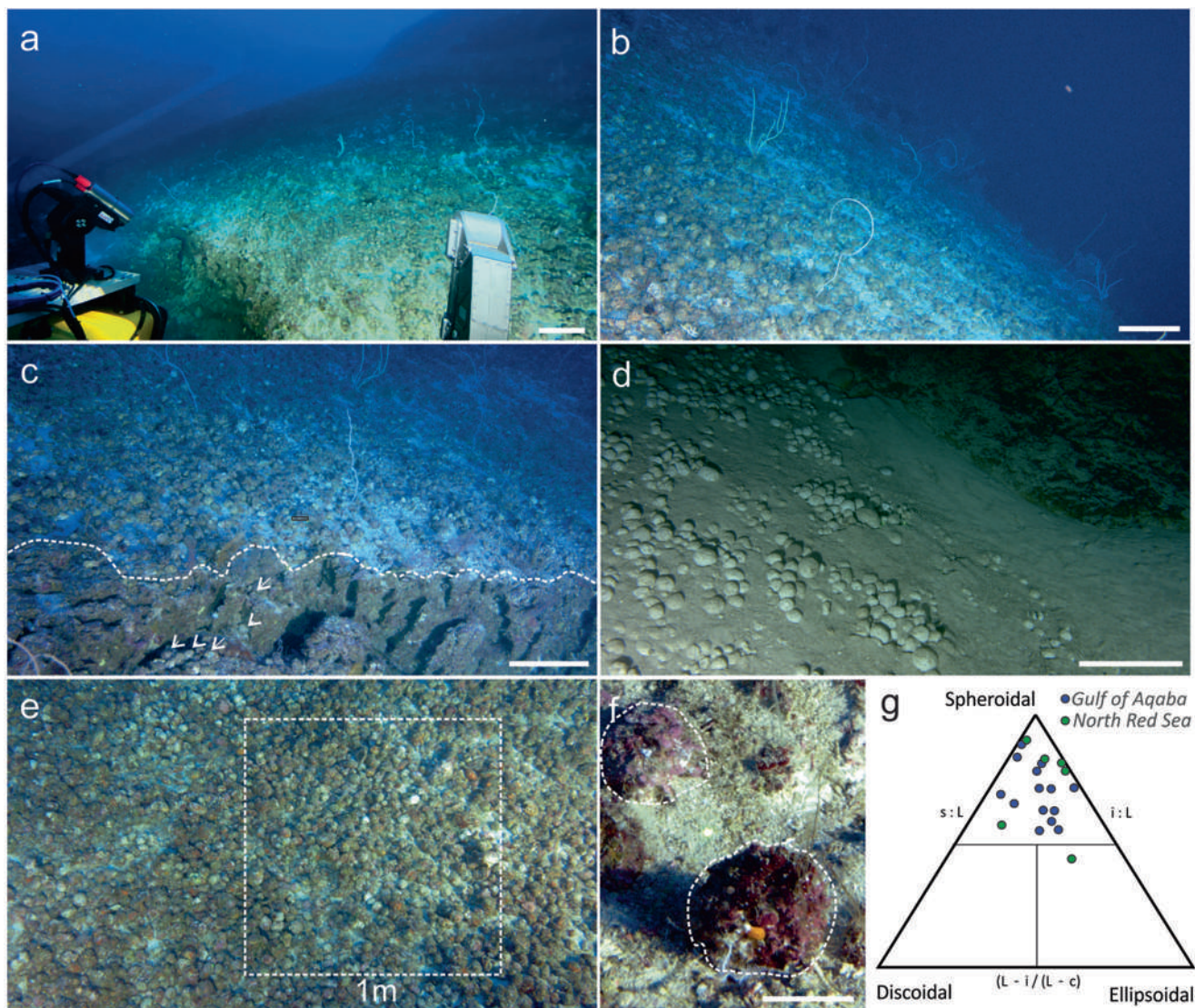
Fig. 2 The NEOM FAN beds. a FANs on a flat seafloor with a cover ranging between 75 and 100% (transect NTN0170, 90 m). Scale bar = 50 cm, refers to seafloor. **b** FANs on a gently sloping seafloor with a cover ranging between 75 and 100% (transect NTN0035, 100 m). Scale bar = 50 cm. **c** The external limit of the shelf with an abrupt shelf break (dashed line) (transect NTN0181, 118 m). Some FANs have fallen over the edge (white arrows). Scale bar = 50 cm. **d** FANs fall and partially sunk into very fine sediment (transect NTN0029, 170 m). Scale bar = 50 cm. **e** Top view of a FAN bed with 1m² inset (transect NTN0043, 80 m). 1 m side dashed quadrat to scale. **f** Close up of two FANs (dashed lines) (transect NTN0043, 80 m). Scale bar = 5 cm. **g** Ternary plot of the FANs shape.

3) show that FANs develop under a wide range of conditions, as already indicated by Matzuda and Iryu[11] although measured temperature ranges for Japan are quite different from the ones in this study. Salinity values are typical for GoA and NERS, whereas temperature values are unevenly distributed, showing a general seasonal trend also in the mesophotic zone, this in agreement with previous findings at least for the GoA[36]. Moreover, the FANs are found over quite a broad depth range where expected temperature range is wide[11]; this paper.

The NEOM mesophotic FAN beds occur on flat (Fig. 2a) or gently sloping (Fig. 2b) seafloor at the external limit of the continental shelf, which can end abruptly (dashed line, Figs. 2c and 5a). There, FANs fall off the edge (Fig. 5a), and possibly roll down slope (Fig. 5b) into the basin, down to at least 425 m (NTN0050-10, Supplementary Table 3) where they eventually accumulate on finer sediment and stop accreting (Fig. 5c). Samples collected at this depth were dead (Supplementary Table 3, gray lines). Moreover, this depth is beyond the

bathymetric tolerance of the organisms that build the nodules (arrows, Fig. 2c, d and Supplementary Table 3) range[16,37]. Unlike mesophotic corals, which are mostly attached to the substrate, we speculate that the spheroidal and sub-spheroidal FANs readily roll along the shelf and down-slope into waters deeper than the mesophotic. Few studies exist on hydraulic behavior of nodules[38–40]. Spheroidal and sub-spheroidal particles, as in our case, are more easily transported because they can roll, especially if associated with coarse sediments. In our study area, the coverage and density of nodules were comparable among study sites (Supplementary Table 1), and although the FANs seem to be partially buried in soft sediment, we can speculate that both currents and bioturbation roll the bioconstructions across the shelf, as is the case for rhodoliths[41,42]. Once the FANs reach the shelf edge, where the seafloor drops away steeply, gravity alone will transport the nodules down slope (Fig. 5). We contend that these transport mechanisms observed in our study area hold for the wider Gulf of Aqaba and Red Sea where the shelf morphology
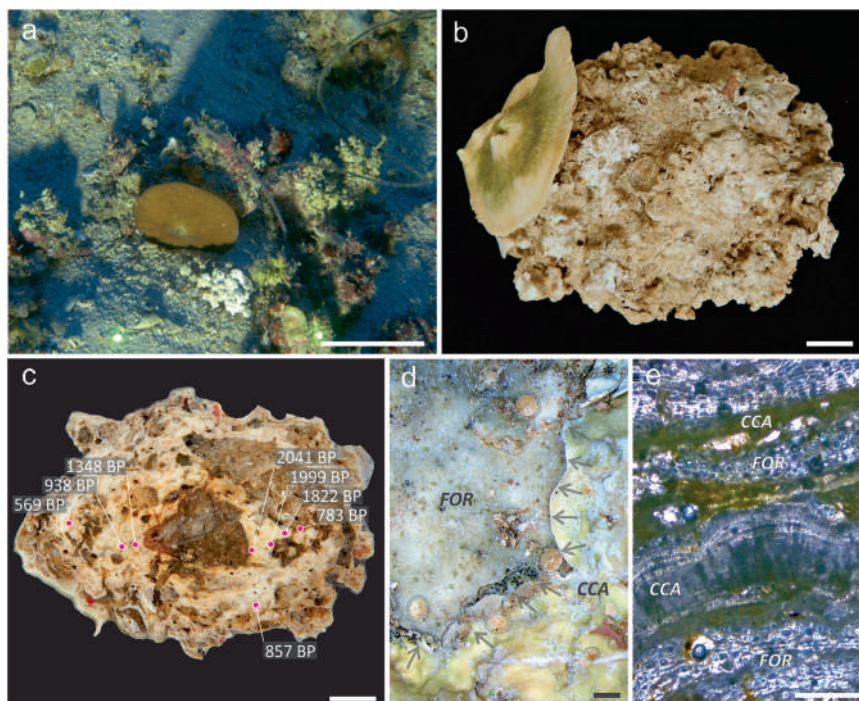
Fig. 3 The sample FAN NTN0035-17A. a FAN NTN0035-17A in situ as it was before the sampling. On the surface, at least one specimen of zooxanthellate hard coral genus *Leptoseris* is visible. Pink crusts are living CCA. Scale bar = 4 cm. **b** FAN NTN0035-17A after drying in the laboratory. On the surface, one large specimen of zooxanthellate hard coral genus *Leptoseris* is visible. Scale bar = 1 cm. **c** Half of the FAN NTN0035-17A after the cutting. The evident nucleus is recognizable at the core. The layering structure is evident around the core. Radiocarbon dating as years BP are reported (Supplementary Table 3). Scale bar = 1 cm. **d** A detail of the surface of FAN NTN0035-17A. FOR is for encrusting foraminifers, CCA is for crustose coralline algae. Gray arrows indicate that CCA crusts overlap, in this case, the layer of encrusting foraminifers. Dashed circles indicate the occurrence of other benthic foraminifers (*Amphistegina lobifera*). Scale bar = 500 μm. **e** A detail of a thin section prepared from FAN NTN0035-17A that shows the layered inner structure, with the alternation of encrusting foraminifers (FOR) and crustose coralline algae (CCA). Scale bar = 500 μm.
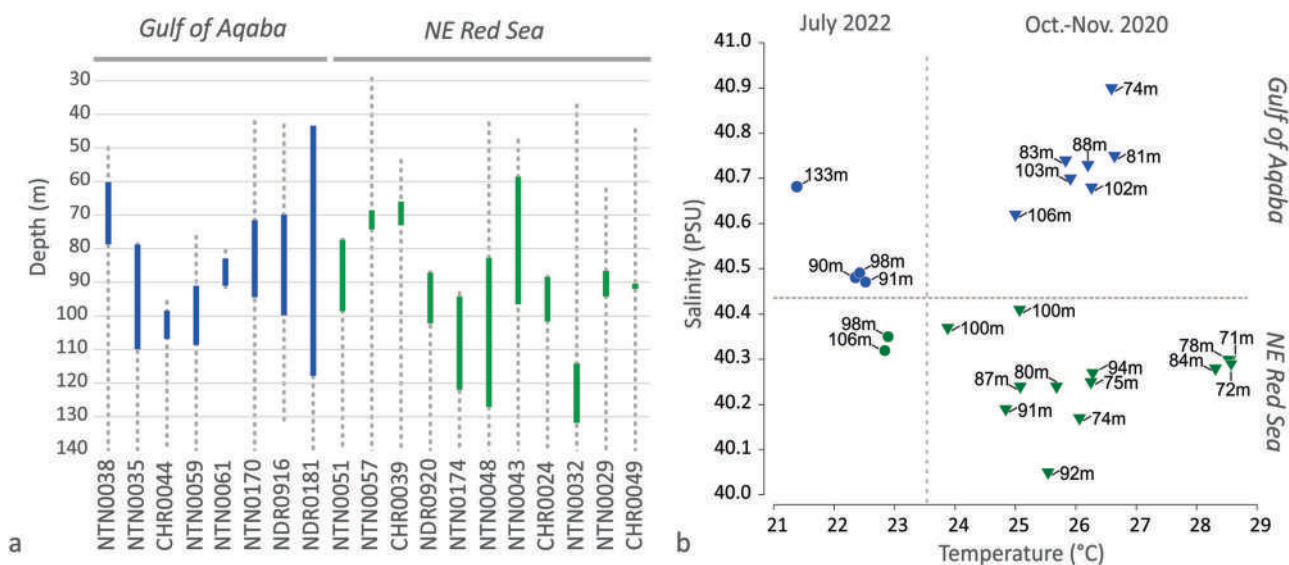

Fig. 4 Depth intervals at which FAN beds occur, and oceanographic data collected at FANs sampling site (S1, Supplementary Table 1). a Bathymetry of FANs beds, thick blue lines for Gulf of Aqaba, green thick lines for the NE Red Sea. The dashed line indicates the full extension of the video transect. **b** Salinity and temperature data collected in correspondence of the sampling sites. Blue for Gulf of Aqaba, green for NE Red Sea. Triangles for October-November 2020 expedition, circles for July 2022 expedition. Horizontal dashed line separates Gulf of Aqaba from NE Red Sea samples; vertical dashed line separates July 2022 from October-November 2020 samples.
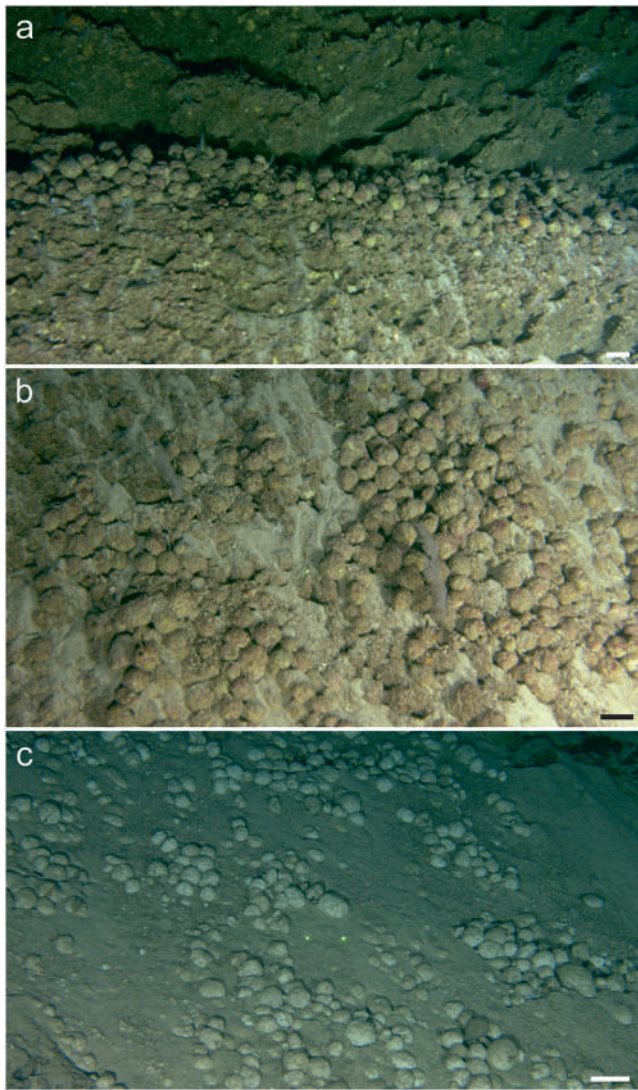
Fig. 5 The spatial and temporal rolling dynamic of FANs (transect NTN0029). Scale bars = 10 cm. a The FANs at the external limit of the edge tend to accumulate (94 m). **b** Some of the FANs can roll down. They stay hanging on the complex surface that the substrate has along the slope and partially still alive (140 m). **c** If FANs continue to roll down, they turn completely white, because of the death of accreting taxa, and partially sink into fine sediments (425 m).

is similar. Few such mechanisms were known for nodules in general, and in the Red Sea, in particular, save for episodic underwater landslides, which are both rare and spatially limited[25].

An active, mesophotic, foralgal carbonate factory has already been reported from the Red Sea[17], but in the form of encrusting build-ups. Our results confirm that the foralgal carbonate factory is active in the mesophotic of the Red Sea, but in a new unexpected form of free-rolling nodules. This represents a novelty and is a noteworthy addition to the tropical carbonate factory[43,44].

Carbonate budget. The habitat Suitability Model (Fig. 6) calculated a potential extension of the FAN beds of 6.27 km^2 ($P > 0.75$, Supplementary Table 4) out of~ 95 km^2, covering at least the 6% of the available shelf along the NEOM coast between 58.6 and 131.8 m of water depth.

The calculated carbonate storage for NEOM FANs ranges from 1.2 to 27.2 kg m^2 (if nodules = 50*m^2) and 6.9 and 156.3 kg m^2

(if nodules = 287*m^2). The total gross carbonate production rate ranges between 0.5 and 66 g m^2 yr^{-1}. Based on the HSM results, the total calcium carbonate currently placed where the seafloor is expected to host FANs ranges between 7.5 and 979.6 megatons. The mesophotic FAN beds of NEOM represent an unexpected and laterally extensive facies belt in the Red Sea that plays an important role in the long-term carbonate budget of the basin. Japan FANs occur on a flat area of 6 km^2 between 61 and 105 m[12], but the authors neither indicate the occurrence of a bed and its extension, nor gave some quantitative indication on the density or coverage of the FANs.

Other mesophotic nodules, such as rhodoliths, have a higher carbonate production rate (0.3 up to 1.07 kg m^2 yr^{-1})[45] but they seem absent from the NEOM area. In the tropics, shallow water coral reefs (0.9–2.7 kg m^2 yr^{-1})[46] are more productive than the ones considered as mesophotic, but data in this case are available only from Caribbean area[33,34]. Moreover, in the Caribbean, mesophotic corals grow slowly, are patchy on the seabed, and therefore represent only limited carbonate repositories[33,34].

Despite FANs distribution and carbonate production are one/two orders of magnitude lower than other nodules, such as rhodoliths, FANs (1) represent unique mesophotic nodules along the NEOM coast contributing to increased complexity of mesophotic environments and biodiversity, and (2) store thousands of tons of calcium carbonate that should be considered when modeling carbonate budget of a region and possible implication under the scenario of climate change. In fact, data on the benthic carbonate factory, such as FAN beds, are fundamental for understanding how carbonate deposition responds to environmental conditions such as oceanographic and atmospheric CO_2 concentrations, both in the past and into the future. Moreover, calcium carbonate production emits CO_2, but, at the same time, is responsible for the burial of C_{inorg}[47]. Consequently, mesophotic benthic habitats such as FANs beds, herein described for the first time in the NEOM area, should be considered in the modeling of such mechanisms, as they are extensive and productive carbonate factories.

Material and methods
Data for this study (Supplementary Tables 1 and 2) was collected during the NEOM-OceanX "Deep Blue Expedition" aboard the M/V OceanXplorer, between October and November 2020, and in June 2022 in the NEOM area, on the Saudi Arabian coast (GoA and NERS). The benthic video footage was recorded by: (a) an ARGUS Mariner XL 108 ROV (Chimaera, CHR) equipped with Kongsberg HIPaP 501 USBL (Ultra-Short Baseline), Sonardyne Sprin INS (Inertial Navigation System) with integrated DVL (Doppler Velocity Logger), HDTV 1080p F/Z Color camera, and two Shilling T4 hydraulic manipulator, and (b) two Triton 3300/3 submersibles (Neptune, NTN, and Nadir, NDR) equipped with Sonardyne Ranger Pro 2 USBL, two parallel-aligned green scaling lasers providing 10 cm scale, and a Schilling T4 hydraulic manipulator. Chimaera and Neptune are both equipped with Arctic Rays EagleRay 4 K cameras and 4 K Atmos Shogun monitors. Nadir is equipped with a Wide-Angle Red DSMC2 Helium 8 K Canon CN-E15.5–47 mm lens and a macro Red DSMC2 Helium 8 K Nikon ED 70–180 mm F4.5–5.6D.

Water column data was collected using a Sea-Bird Electronics 911plus CTD cast from the vessel and with RBR Maestro CTD mounted on ROV or submersible (on NTN for 7 dives and CHR for 29 dives). Measurements for temperature, salinity and oxygen concentration were taken every minute for the duration of the dives. Data from a total of 21 transects was used for this study (14 NTN, 3 NDR and 4 CHR, Fig. 1, Supplementary Table 1), moving from the continental slope up to the shelf, between 705.4 and
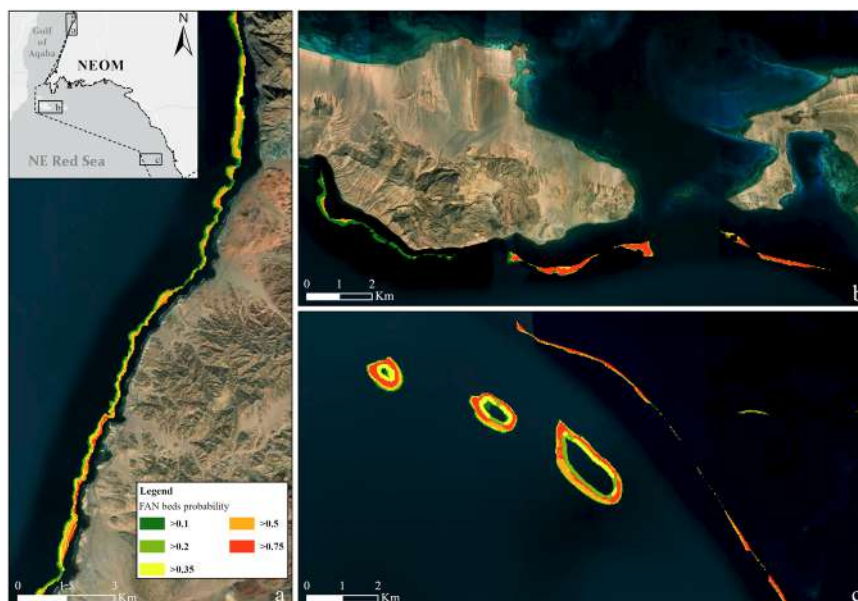
Fig. 6 Maps showing the results of the Habitat Suitability Model (HSM) of FAN beds for the NEOM region. a FAN HSM for the area of Magna, along the Gulf of Aqaba coast. **b** FAN HSM in the NE Red Sea, around Tiran Island. **c** FAN HSM for NE Red Sea, in the area of Sila Island. ESRI World Image Basemap, source: Esri, Maxar, Earthstar Geographics.

12.6 m of water depth. Video transects were georeferenced using USBL dataset and plotted in ArcGIS Pro 3.0 software. Videos were processed to detect the occurrence of FANs on the shelf, providing spatial information about their occurrence and distribution. The bathymetric intervals at which nodules occur were manually extracted by video transects (Supplementary Table 1). Environmental data have been extracted from the CTD dataset specifically for the interval at which nodules have been collected (Supplementary Table 2). Video-frames have been manually extracted to describe and quantify the FANs and the beds (Supplementary Tables 1 and 2). Nodule cover was evaluated by using 4 percentage cover classes (0–25, 25–50, 50–75, 75–100) *per* videoframe. Moreover, video-frames when the cameras were perpendicular to the seafloor were considered to calculate the number of nodules *per* square meter (Fig. 3 and Supplementary Table 2).

Nodules have been collected by hydraulic manipulators mounted on ROV and submersibles. Nodules have been collected from different localities: please refer to Fig. 1 and Supplementary Table 2 for details. Nodule shape was evaluated by measuring Long (L), Intermediate (I) and Short (S) axes with a manual caliber ($n = 20$) (Supplementary Table 2). The results were plotted in Sneed and Folk's[48] pebble shape diagram using Tri-Plot[49] (Fig. 2g). The volume of each nodule was calculated using the formula:

$$V = 4/3 * L/2 * I/2 * S/2 * \pi. \tag{1}$$

The mass of each nodule was measured (Supplementary Table 1), and the density was calculated as the *ratio* between volume and mass (Supplementary Table 2). A Pearson test (Microsoft Excel) has been computed to test their correlation.

Five samples (Supplementary Table 2, green lines) were glued in epoxy resin and cut. One-half was used to prepare thin sections with the aim of describing the inner structure and identifying the main components using an optical microscope for the identification of the main taxa and comparison with previous literature data for foraminifers (Fig. 3). A qualitative evaluation of their abundance was done under the microscope.

The other half was used for dating (Fig. 3c and Supplementary Fig. 1). Radiocarbon ages were determined from biogenic carbonate made of foraminifers or CCA collected in different inner positions of the nodule, after verifying their preservation by Scanning electron Microscope observations (Fig. 2g). Some additional samples were collected from endolithic bivalves and sediment filling the inner cavities (Supplementary Table 3). Samples ($n = 5$) were sent to Alfred-Wegener-Institute (Helmholtz, Germany) for analysis by accelerator mass spectrometry with the MICADAS system. The results have been calibrated against the current marine calibration curve (Marine 20)[50] using CALIB 8.2 online platform[51] and considering the regional marine radiocarbon reservoir age correction (ΔR of -14 ± 16 ^{14}C years)[25]. [14]C ages are reported as years Before Present (yrs BP, present = AD 1950), and as calibrated ages (cal yrs BP) with 2σ error (Supplementary Table 3). We then calculated the accretion rates considering the distance (mm) from dated points and surface of the nodule (Supplementary Table 3).

Habitat Suitability Models (HSM), are one of the existing tools which allow us to combine known presence data (this paper) with continuous layers of environmental and geomorphometric variables, in order to estimate the suitable areas for the species or assemblages of interest. Maximum Entropy (MaxEnt) version 3.4.4 software[52] was used to create a suitability distribution model for the nodules. The bathymetric dataset used for the modeling was collected during the OceanX-NEOM Deep Blue Expedition and merged with the bathymetry by ref. [53] for the GoA. Twenty-six geomorphometric parameters were extracted from the bathymetry using ArcGIS and SAGA GIS[54], and used as initial predictor variables for the suitability model (Supplementary Table 4). Seafloor environmental conditions were interpolated from the RBR data collected from ROV and submersible dives. The DIVA (Data-Interpolating Variational Analysis)[55] gridding function was used in OceanDataView[56] to interpolate within narrow depth bands. Depth bands were chosen to ensure sufficient resolution within the FANs bed depth range, while ensuring there are adequate measurements within the band to interpolate with confidence (18 bands were created with the following resolutions: intervals of 10 m between 50–150 m; intervals of 50 m

between 0–50 m and 150–300 m; intervals of 100 between 300–600 m; a single band for 600–1700 m). Rasters were generated for each depth band by importing the points to ArcMap and interpolating using the kriging function, before merging to create three continuous rasters for the entire depth range (temperature, oxygen concentration, and salinity).

MaxEnt uses a maximum likelihood algorithm which aims to provide the most dispersed distribution within the provided constraints. A correlation analysis was conducted between all predictors in R (version 4.1.2) in order to identify pairs of correlated variables. Among all pairs of variables with $r^2 > 0.7$, the percent contribution to the model, as calculated by MaxEnt, was used to determine which variables to keep (Supplementary Table 4). The reduced predictor variable set included twelve variables (Supplementary Table 4). The final dataset contained 2378 FANs presence points. After removing duplicated points to avoid location bias, 93 presence points were considered (Supplementary Table 4). The model was run in MaxEnt using 70% of the data (66 points) to train the model, and 30% (27 points) as test data. The model was run 10 times using bootstrapping. Only hinge features were enabled, and the regularization multiplier was set to 2.5 to create a smoother and more generalized model[57,58]. All other MaxEnt settings were kept as default. We assessed the model using the Area Under the receiver operating Curve (AUC) value, which is a common measure of model performance, the average training model AUC is 0.9962 and the average test model AUC is 0.9960, which indicates a high performance of the model within the study area. The most important predictor variables are depth (44.6% contribution), temperature (31.9%) and Vector Ruggedness measure (VRM), a proxy for surface complexity (12.1%) (Supplementary Table 4). Lastly, we calculated the FANs carbonate budget. The actual amount of carbonate was calculated as the medium mass of nodule * the number of nodule in 1 m². This value was then extended to the whole area obtained by HMS. Finally, the total gross carbonate production rate was calculated as the amount of carbonate per square meter divided for the maximum dating resulting from the C[14] measures.

Reporting summary. Further information on research design is available in the Nature Portfolio Reporting Summary linked to this article.

Data availability

References
1. Reid, P. R. & Macintyre, I. G. Foraminiferal-algal nodules from the eastern Caribbean: growth history and implications on the value of nodules as paleoenvironmental indicators. *PALAIOS* **3**, 424 (1988).
2. Riosmena-Rodríguez, R., et al. Rhodolith/maerl beds: a global perspective. Coastal Research Library, https://doi.org/10.1007/978-3-319-29315-8_11.
3. Steller, D. L. & Caceres-Martinez, C. Coralline algal rhodoliths enhance larval settlement and early growth of the Pacific calico scallop *Argopecten ventricosus*: Marine Ecol Prog. Series **396**, 49–60 (2009).
4. Nelson, W. A. Calcified macroalgae critical to coastal ecosystems and vulnerable to change: a review. *Mar. Freshw. Res.* **60**, 787–801 (2009).
5. Harvey, A. S. et al. The distribution, significance and vulnerability of Australian rhodolith beds: a review. *Mar. Freshw. Res* **68**, 411–428 (2016).
6. Cornwall, C. E. et al. Global declines in coral reef calcium carbonate production under ocean acidification and warming. *Proc. Natl Acad. Sci. USA* **118**, e2015265118 (2021).
7. Rendina, F. et al. The scientific research on rhodolith beds: a review through bibliometric network analysis. *Ecol. Inform.* **70**, 101738, (2022).
8. Loya et al. *Mesophotic Coral Ecosystems* (Springer Cham, 2019).
9. Prager, E. J. & Ginsburg, R. N. Carbonate nodule growth on Florida's outer shelf and its implications for fossil interpretations. *Palaios* **4**, 310–317 (1989).
10. Minnery, G. Crustose coralline algae from the Flower Garden Banks, Northwestern Gulf of Mexico: controls on distribution and growth morphology. *J. Sed. Petrol.* **60**, 992–1007 (1990).
11. Matsuda, S. & Iryu, Y. Rhodoliths from deep fore-reef to shelf areas around Okinawa-jima, Ryukyu Islands, Japan. *Mar. Geol.* **282**, 215–230 (2011).
12. Bassi, D. et al. Deep-water macroid beds of the Ryukyu Islands, Japan: Encrusting acervulinids as ecosystem engineers. *J. Coat. Res.* **35**, 463–466 (2019).
13. Bassi, D. et al. Recent macroids on the Kikai-jima shelf, Central Ryukyu Islands, Japan. *Sedimentology* **59**, 2024–2041 (2012).
14. Hottinger, L. & Levinson, G. Cementation of reefs in the Gulf of Elat (Red Sea) by Acervulinid Foraminifera. In: Abstract Lecturer of the 10th International Congress on Sedimentology vol I, Jerusalem (ed Friedman, G. M.), pp. 315, (1978).
15. Hottinger, L. Neritic macroid genesis, an ecological approach.In *Coated Grains* (ed. Peryt, T. M.), 38–55 (Springer-Verlag, 1983).
16. Reiss, Z. & Hottinger, L. The Gulf of Aqaba: ecological micropaleontology. *Ecological Studies* Vol. 50. 354 pp. (Springer-Verlag, 1984).
17. Dullo, W. F. et al. The foralgal crust facies of the deeper fore reefs in the Red Sea: a deep diving survey by submersible. *Geobios* **23**, 262–281 (1990).
18. Sheppard, C. R. & Sheppard, A. L. S. *Corals and Coral Communities of Arabia*. In Fauna of Saudi Arabia Vol. 12, Natural History Museum, Basle (eds Buttiker, W. and Krupp, F.), pp. 170 (1991).
19. Voolstra, C. R. & Berumen, M. L. *Coral Reefs of the Red Sea* 179 pp (Springer, 2019).
20. Fricke, H. On the pathways of the "Pola" expeditions. Deep-water exploration of the Red Sea by submersible. In *Deep Sea and Extreme Shallow-water Habitats: Affinities and Adaptations* (eds. Uiblein, F., Ott, J., Stachowitsch, M.), Biosystematics and Ecology Series 11, 67–89 (1996).
21. Qurban, M. A. et al. In-situ observation of deep water corals in the northern Red Sea waters of Saudi Arabia. *Deep-Sea Res. I Oceanogr. Res. Pap.* **89**, 35–43 (2014).
22. Chimienti, G. et al. A new species of *Bathypathes* (Cnidaria, Anthozoa, Antipatharia, Schizopathidae) from the Red Sea and its phylogenetic position. *ZooKeys* **1116**, 1–22 (2022).
23. Maggioni, D. et al. The First Deep-Sea Stylasterid (Hydrozoa, Stylasteridae) of the Red Sea. *Diversity* **14**, 241 (2022).
24. Purkis, S. J. et al. Discovery of the deep-sea NEOM Brine Pools in the Gulf of Aqaba, Red Sea. *Commun. Earth. Environ.* **3**, 146 (2022a).
25. Purkis, S. J. et al. Tsunamigenic potential of an incipient submarine landslide in the Tiran Straits. *Geophys. Res. Lett.* **49**, e2021GL097493 (2022b).
26. Terraneo, T. I. et al. The complete mitochondrial genome of *Dendrophyllia minuscula* (Cnidaria: Scleractinia) from the NEOM region of the Northern Red Sea. *Mitochondrial DNA 289* **7**, 848–850 (2022). Part B.
27. Terraneo, T., et al. From the shallow to the mesophotic: a characterization of Symbiodiniaceae diversity in the Red Sea NEOM region. *Front. Marine Sci.* **10** (2023).
28. Humphreys, A. F. et al. *Amphistegina lobifera* foraminifera are excellent bioindicators of heat stress on high latitude Red Sea reefs. *Coral Reefs* **41**, 1211–1223 (2022).
29. Rasul, N. M. A., & Stewart I. C. F. *Oceanographic and Biological Aspects of the Red Sea* 550 pp. (Springer, 2018).
30. Foster, M. S. Rhodoliths: between rocks and soft places. *J. Phycol.* **37**, 659–667 (2001).
31. Littler, M. M., Littler, D. S. & Hanisak, M. D. Deep-water rhodolith distribution, productivity, and growth history at sites of formation and subsequent degradation. *J. Exp. Mar. Biol. Ecol.* **150**, 163–182 (1991).
32. Caragnano, A., Basso, D. & Rodondi G. Growth rates and ecology of coralline rhodoliths from the Ras Ghamila back reef lagoon, Red Sea. *Marine Ecol.* **37**, 713–726 (2016).
33. Weinstein, D. K. et al. Coral growth, bioerosion, and secondary accretion of living orbicellid corals from mesophotic reefs in the US Virgin Islands. *Mar. Ecol. Prog. Ser.* **559**, 45–63 (2016).
34. Groves, S. H. et al. Growth rates of *Porites astreoides* and *Orbicella franksi* in mesophotic habitats surrounding St. Thomas, US Virgin Islands. *Coral Reefs* **37**, 345–354 (2018).
35. Lambeck, K. et al. Sea level and shoreline reconstructions for the Red Sea: isostatic and tectonic considerations and implications for hominin migration out of Africa. *Quat. Sci. Rev.* **30**, 3542–3574 (2011).
36. Nir, O., Gruber, D. F., Shemesh, E., Glasser, E. & Tchernov, D. Seasonal mesophotic coral bleaching of *Stylophora pistillata* in the North Red Sea. *PloS One* **9**, e84968 (2014).

37. Littler, M. M., Littler, D. S. Models of tropical reef biogenesis: the contribution of algae. in *Progress in Phycological Research* (eds Round, F. E., Chapman, V. J.) 323–364 (Biopress, 1984).

38. Bosence, D. W. J. Description and classification of rhodoliths (rhodoids, rhodolites). In *Coated Grains* (ed Peryt, T. M.) 217–224 (Springer, 1983).

39. Basso, D. & Tomaselli, V. Paleoecological potentiality of rhodoliths: a Mediterranean case history. *Boll. Soc. Paleontol. Ital.* **2**, 17–27 (1994).

40. Jardim, V. L. et al. Quantifying maerl (rhodolith) habitat complexity along an environmental gradient at regional scale in the Northeast Atlantic. *Mar. Environ. Res.* **181**, 105768 (1999).

41. Marrack, E. C. The relationship between water motion and living rhodolith beds in the southwestern Gulf of California, Mexico. *Palaios* **14**, 159–171 (1999).

42. O'connell, L. G. et al. Reevaluation of the inferred relationship between living rhodolith morphologies, their movement, and water energy: Implications for interpreting palaeoceanographic conditions. *Palaios* **35**, 543–556 (2021).

43. Purkis, S. J., Harris, P. M. & Ellis, J. Patterns of sedimentation in the contemporary Red Sea as an analog for ancient carbonates in rift settings. *J. Sed. Res.* **82**, 859–870 (2012).

44. Reijmer, J. J. G. Marine carbonate factories: review and update. *Sedimentology* **68**, 1729–1796 (2021).

45. Amado-Filho, G. M. et al. Rhodolith beds are major CaCO3 bio-factories in the tropical South West Atlantic. *PLoS One* **7**, e35171 (2012).

46. Vecsei, A. A new estimate of global reefal carbonate production including the fore-reefs. *Glob. Planet. Change* **43**, 1–18 (2004).

47. Saderne, V. et al. Role of carbonate burial in Blue Carbon budgets. *Nat. Commun.* **10**, 1106 (2019).

48. Sneed, E. D. & Folk, R. L. Pebbles in the lower Colorado River, Texas, a study in particle morphogenesis. *J. Geol.* **66**, 114–150 (1958).

49. Graham, D. J. & Midgley, N. G. Graphical representation of particle shape using triangular diagrams: an Excel spreadsheet method. *Earth Surf. Proc. Land.* **25**, 1473–1477 (2000).

50. Heaton, T. J. et al. Marine20 - the marine radiocarbon age calibration curve (0–55,000 cal BP), simulated data for IntCal20. PANGAEA (2020).

51. Stuiver, M., Reimer, P. J. & Reimer, R. W. *CALIB 8.2*, accessed 15 November 2022. http://calib.org.

52. Phillips, S. J., Dudík, M. & Schapire, R. E. Maxent software for modeling species niches and distributions (Version 3.4.1). Available from: http://biodiversityinformatics.amnh.org/open_source/maxent/. Accessed 26 February 2023.

53. Ribot, M. et al. Active faults' geometry in the Gulf of Aqaba, southern Dead Sea Fault, illuminated by multibeam bathymetric data. *Tectonics* **40**, e2020TC006443 (2021)

54. Conrad, O. et al. System for automated geoscientific analyses (SAGA) v. 2.1.4. *Geosci. Model Dev.* **8**, 1991–2007 (2015).

55. Barth, A. et al. DIVAnd-1.0: n-dimensional variational data analysis for ocean observations. *Geosci. Model Dev.* **7**, 225–241 (2014).

56. Schlitzer, R. *Ocean Data View* https://odv.awi.de (2021).

57. Elith, J., Kearney, M. & Phillips, S. The art of modelling range-shifting species. *Methods Ecol. Evol.* **1**, 330–342 (2010).

58. Merow, C., Smith, M. J. & Silander, J. A. Jr A practical guide to MaxEnt for modeling species' distributions: what it does, and why inputs and settings matter. *Ecography* **36**, 1058–1069 (2013).

Author contributions

V.A.B. and F.B. conceived the research and wrote the manuscript. V.A.B. conducted the FANs structure, dating and carbonate budget analyses, F.B. the ecological dataset analyses and M.K.B.N. and F.M. the HSM modelling analyses. S.J.P. collected data, contributed to the data analysis and edited the manuscript. F.B, F. M., T.I.T., S.V. and G.C. collected data and samples for this research. A.E. was expedition leader of the 2020 Deep Blu Expedition. M.R. and all the other authors revised the manuscript.

Competing interests

The authors declare no competing interests.

Additional information

Supplementary information The online version contains supplementary material available at https://doi.org/10.1038/s43247-023-00944-w.

Correspondence and requests for materials should be addressed to Valentina Alice Bracchi.

Peer review information *Communications Earth & Environment* thanks Victor Jardim, Laura O'Connell and the other, anonymous, reviewer(s) for their contribution to the peer review of this work. Primary Handling Editors: Olivier Sulpis and Clare Davis. A peer review file is available.

Reprints and permission information is available at http://www.nature.com/reprints

Publisher's note Springer Nature remains neutral with regard to jurisdictional claims in published maps and institutional affiliations.